Exact investigation of the electronic structure and the linear and nonlinear optical properties of conical quantum dots

M. Dezhkam and A. Zakery*

Department of Physics, College of Sciences, Shiraz University, Shiraz 71454, Iran

**Corresponding author: zakeri@susc.ac.ir*

Received May 2, 2012; accepted June 20, 2012; posted online October 24, 2012

Intersubband linear and third-order nonlinear optical properties of conical quantum dots with infinite barrier potential are studied. The electronic structure of conical quantum dots through effective mass approximation is determined analytically. Linear, nonlinear, and total absorption coefficients, as well as the refractive indices of GaAs conical dots, are calculated. The effects of the size of the dots and of the incident electromagnetic field are investigated. Results show that the total absorption coefficient and the refractive index of the dots largely depend on the size of the dots and on the intensity and polarization of the incident electromagnetic field.

OCIS codes: 190.4720, 160.4760.
doi: 10.3788/COL201210.121901.

Quantum dots (QDs) are quasi-zero-dimension systems, the carriers of which are confined in all the three spatial dimensions. These quantum systems, which were first studied by Esaki in 1970[1], are described as "artificial atoms" because of their δ-function-like density of states[2].

Unlike bulk crystals with band energies, QDs have discrete subbands because of their three-dimensional (3D) confinements. Intersubband transitions result in physical and optical properties and make QDs useful for infrared (IR) optoelectronic devices. The absorption coefficient (AC) and refractive index (RI) of the host material change because of the considerably large dipole matrix element and the low energy of intersubband transitions. In particular, the enhancement of nonlinear optical properties is important in QDs. Nonlinear properties depend on incident optical intensity; thus, at high incident intensities, the nonlinear properties should be considered.

Researchers have recently investigated the electronic structure and the linear and nonlinear optical properties of different shapes of QDs, such as the box-shaped[1], parabolic cylinder[3], lens-shaped[4], spherical[5], and disc-like[6] QDs with finite, infinite, or Gaussian confining potential.

Self-assembled InAs/GaAs QDs formed through Stranski–Krastanow growth can be pyramid-shaped[2]. These systems are important for laser applications[7]. Thus, researchers have approximated the pyramids by using cones to obtain the energy levels of conical quantum dots (CQDs)[8−10].

In this letter, a CQD with an infinite barrier potential is considered. The Schrödinger equation in the effective mass approximation is solved analytically to determine the electronic structure of CQDs. Subsequently, the linear, third-order nonlinear, and total AC and RI changes are investigated. Moreover, the dependencies of these optical properties on QD size and on the intensity and polarization of the incident electromagnetic field are studied.

We consider that an electron confined in a CQD has an infinite barrier potential, i.e., $V(\mathbf{r}) = 0$ inside and $V(\mathbf{r}) = \infty$ outside the CQD. To solve this problem analytically, we consider several assumptions, i.e., we deem the potential outside of the QD to be infinite, although in reality, the wavefunctions penetrate into the host material[10]. In the effective mass approximation, the Schrödinger equation for an electron inside the cone is

$$-\frac{\hbar^2}{2m^*}\nabla^2\psi(\mathbf{r}) = E\psi(\mathbf{r}), \tag{1}$$

where $\hbar$ is the Planck's constant divided by 2π, and, m^* is the electron effective mass, E is the energy eigenvalue, and $\psi(\mathbf{r})$ is the eigenfunction of the system. The geometry of the cone is shown in Fig. 1. R', h, and α are the basis radius, height, and apex angle of the cone, respectively. The azimuthal symmetry facilitates the approximation of the cone by means of spherical coordinates. To obtain the approximation, we consider the origin of the frame at the cone apex. The polar axis is the cone axis. $R = (R'^2 + h^2)^{1/2}$ represents the radius of the sphere, a part of which is the cone. The area inside the CQD is specified by $r < R$, $0 \leqslant \varphi \leqslant 2\pi$, and $\theta < \alpha$.

Equation (1) is rewritten by using spherical coordinates, and is separable due to the infinite barrier potential. Thus, the eigenfunction $\psi(\mathbf{r})$ can be written as

$$\psi(r, \theta, \varphi) = Nf(r)g(\theta)\mathrm{e}^{\mathrm{i}m\varphi}, \tag{2}$$

where N is the normalization constant. To create a single-valued azimuthal part, m must be an integer if the full azimuthal range is allowed ($|m| = 0, 1, 2, \cdots$).

Substituting Eq. (2) into Eq. (1) gives radial and θ equations. The solutions of the θ equation are associated Legendre functions of the first and second kinds, i.e., $P_\nu^m(\cos\theta)$ and $Q_\nu^m(\cos\theta)$. As mentioned previously, we derive $\cos\alpha \leqslant \cos\theta \leqslant 1$. $Q_\nu^m(\cos\theta)$ diverges at $\cos\theta = 1$ and is thus omitted[11]. The associated Legendre function $P_\nu^m(\cos\theta)$ is regular at $\cos\theta = 1$ and for $|\cos\theta| < 1$, but singular at $\cos\theta = -1$ unless ν is an integer. In this instance, $\cos\theta = -1$ is excluded; thus, ν is real but nonintegral[12]. The spherical Bessel functions of the first and second kinds are solutions to the radial equation. The spherical Bessel functions of the second kind, which are called "spherical Neumann functions,"

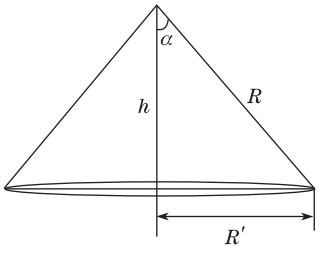

Fig. 1. Geometry of CQD.

are omitted because of their singularity at the origin[11]. Therefore, the wavefunction becomes

$$\psi(r,\theta,\varphi) = Nj_\nu(kr)P_\nu^m(\cos\theta)\mathrm{e}^{\mathrm{i}m\varphi}, \tag{3}$$

where $k = (2m^*E/\hbar^2)^{1/2}$. Separation constants ν and k are determined by the boundary conditions. The CQD is limited by two surfaces. Thus, the wavefunction $\psi(\mathbf{r})$ should vanish at $\theta = \alpha$ and $r = R$ to satisfy the boundary conditions. Therefore,

$$P_\nu^m(\cos\alpha) = 0, \tag{4}$$

$$j_\nu(x) = 0, \tag{5}$$

where $x = kR$. Eigenvalues E and eigenfunctions $\psi(\mathbf{r})$ can be determined by solving these equations.

Figure 2 shows the transition energies of an electron confined in a CQD from the ground to the first excited state as a function of the basis radius R' for the different apex angles of 20°, 25°, 30°, and 45°. In the calculation, $m^* = 0.067m_0$ is used, where m_0 is the electron mass.

To calculate the optical properties of CQD induced by the optical transition between two subbands in the conduction band, we assume that the system is excited by an electromagnetic field polarized along the z direction. Using the compact density matrix formulation of quantum mechanics, the linear and third-order nonlinear AC(RI) are obtained by[1]

$$\alpha^{(1)}(\omega) = \omega\sqrt{\frac{\mu}{\varepsilon_R}}\frac{\sigma_\nu |M_{12}|^2 \hbar\Gamma_{12}}{(E_{21}-\hbar\omega)^2 + (\hbar\Gamma_{12})^2}, \tag{6}$$

$$\alpha^{(3)}(\omega, I) = -\omega\sqrt{\frac{\mu}{\varepsilon_R}}\left(\frac{I}{2\varepsilon_0 n_r c}\right)\frac{\sigma_\nu |M_{12}|^2 \hbar\Gamma_{12}}{\left[(E_{21}-\hbar\omega)^2 + (\hbar\Gamma_{12})^2\right]^2} \cdot\left\{4|M_{12}|^2 - \frac{(M_{22}-M_{11})^2\left[3E_{21}^2 - 4E_{21}\hbar\omega + \hbar^2\left(\omega^2 - \Gamma_{12}^2\right)\right]}{E_{21}^2 + (\hbar\Gamma_{12})^2}\right\}, \tag{7}$$

$$\frac{\Delta n^{(1)}(\omega)}{n_r} = \frac{1}{2n_r^2\varepsilon_0}\frac{\sigma_\nu |M_{12}|^2 (E_{21}-\hbar\omega)}{(E_{21}-\hbar\omega)^2 + (\hbar\Gamma_{12})^2}. \tag{8}$$

$$\frac{\Delta n^{(3)}(\omega)}{n_r} = -\frac{\mu c I}{4n_r^3\varepsilon_0}\frac{\sigma_\nu |M_{12}|^2}{\left[(E_{21}-\hbar\omega)^2 + (\hbar\Gamma_{12})^2\right]^2} \times\left\{4(E_{21}-\eta\omega)|M_{12}|^2 - \frac{(M_{22}-M_{11})^2}{E_{21}^2 + (\eta\Gamma_{12})^2}\left\{(E_{21}-\eta\omega) \times\left[E_{21}(E_{21}-\eta\omega) - (\eta\Gamma_{12})^2\right] - (\eta\Gamma_{12})^2(2E_{21}-\eta\omega)\right\}\right\}, \tag{9}$$

where μ is the permeability of the system, ε_R is the real part of the permittivity, σ_ν is the carrier density, $M_{ij} = |\langle\psi_i|e\hat{z}|\psi_j\rangle|$ is the matrix element of the dipole moment, e is the electronic charge, ψ_i is the eigenfunction of the ith subband given by Eq. (3), $E_{21} = E_2 - E_1$ is the energy difference between these subbands, Γ_{12} is the relaxation rate produced by the electron-phonon interaction and the other collision processes, ε_0 is the permittivity of free space, n_r is the refractive index, c is the speed of light in free space, and I is the incident optical intensity defined as $I = 2\varepsilon_0 n_r c|E|^2$.

The total AC(RI) changes $\alpha(\omega)$, $(\frac{\Delta n(\omega)}{n_r})$ are the sum of the linear and nonlinear ACs(RIs).

Subsequently, we assume a GaAs CQD and then calculate the linear and third-order nonlinear AC and RI changes. The following parameters are used in the calculations: $\varepsilon = 13.18$, $\sigma_\nu = 3\times10^{16}$ cm^{-3}, $n_r = 3.2$, and $\Gamma_{12} = 5\mathrm{ps}^{-1}$[1].

Figures 3(a) and (b) represent the linear, third-order nonlinear, and total AC and RI changes of a CQD as a function of photon energy $\hbar\omega$ for $I = 0.4$ MW/cm^2, a basis radius of R'=10 nm, and an apex angle of $\alpha = \frac{\pi}{4}$[2]. The peak of AC and the zero of RI occur at photon energy of 157.334 meV, which is equal to the energy difference between transition subbands. The linear and third-order nonlinear ACs (RIs) have opposite signs. Therefore, accounting the third-order AC(RI) reduces the total AC(RI). Thus, the third-order AC(RI) should be considered when a strong incident optical intensity is used.

The total AC and total RI of a CQD as a function of photon energy $\hbar\omega$ for $I = 0.4$ MW/cm^2, $\alpha = \frac{\pi}{4}$[2], and for the different basis radii R' =5, 10, 15, 20 nm are plotted in Figs. 4(a) and (b), respectively. As the basis radius increases, the energy difference E_{21} decreases. Consequently, the total AC and total RI exhibit red shifts. The total AC and total RI strongly depend on CQD basis radius. Increasing the CQD basis radius will result in a decrease in AC or an increase in RI.

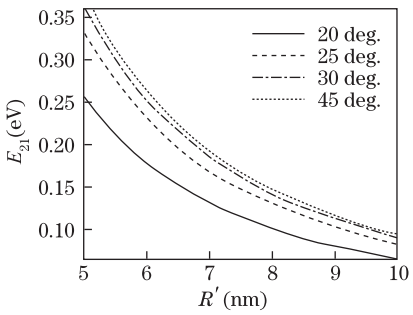

Fig. 2. Transition energies of an electron confined in a CQD from the ground to the first excited state as a function of the basis radius R' for different apex angles.

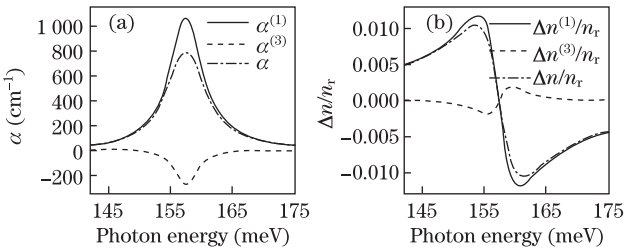

Fig. 3. Linear, third-order nonlinear, and total changes of (a) AC and (b) RI for a CQD with a basis radius of $R' = 10$ nm as a function of photon energy.

The total AC and total RI of a CQD as a function of photon energy $\hbar\omega$ for $I = 0.4$ MW/cm^2, R' =10 nm, and for different apex angles $\alpha = 20, 30, 45$ deg. are plotted in Figs. 5(a) and (b), respectively. As the apex angle decreases, the energy difference E_{21} decreases. Consequently, the total AC and total RI exhibit red shifts. The total AC and total RI strongly depend on the CQD apex angle. Decreasing the CQD apex angle will result in a decrease in AC or an increase in RI.

Shown as Eqs. (6)–(9), in contrast to the linear properties, third-order nonlinear optical properties largely depend on the incident optical intensity. Figures 6(a) and (b) represent the total AC and total RI of a CQD as a function of photon energy $\hbar\omega$ for a basis radius of 10 nm, $\alpha = \frac{\pi}{4}$[2], and for the different incident optical intensities of 0.0, 0.4, 0.6, 0.8, 1.0, and 1.3 MW/cm^2. The resonance peak and zero positions remain constant as the intensity increases, but the total AC and total RI decrease significantly. This condition is accounted by the increase in intensity, which facilitates an increase in nonlinear AC(RI) while linear parts remain constant. Given that the linear and nonlinear parts of AC(RI) have opposite signs, the total AC and total RI decrease. Figure 6(a) shows an absorption saturation that begins at an intensity of 0.8 MW/cm^2. For higher intensity values, the absorption peak splits up into two peaks owing to strong saturation.

We proceed to investigate the effect of incident electromagnetic field polarization on the optical properties of CQD. Specific to this case, we assume that the electromagnetic field is polarized along the x direction. Figures 7(a) and (b) represent the total ACs and total RIs of a CQD as a function of photon energy $\hbar\omega$ with a basis radius of 10 nm, $\alpha = \frac{\pi}{4}$[2], and $I = 0.4$ MW/cm^2 for the electromagnetic field polarization along the z and x directions. Figure 7(a) shows that the position of the absorption peak for the x-polarization is at 94.74 meV, which is lower than that of z-polarization because of the lower transition energy (E_{21}). The electromagnetic field polarization and selection rules produce a transition between the ground and second excited states for the z-polarization. For x-polarization, the transition occurs between the ground and first excited states, the transition energy of which is lower than that of the former.

As regarding Eqs. (3)–(5), we find that the wavefunctions $\psi(\mathbf{r})$ and the energy eigenvalues E depend on the magnetic quantum number m. The matrix elements of the dipole moment M_{ij} become nonzero only

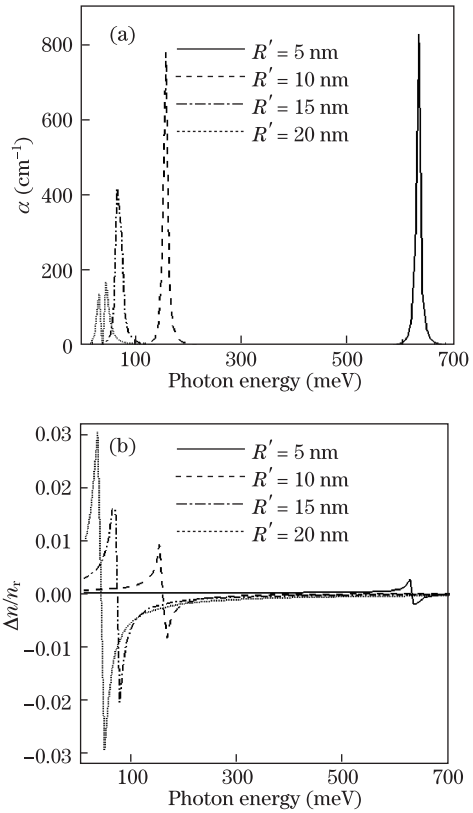

Fig. 4. (a) Total AC and (b) total RI of a CQD versus photon energy for different CQD basis radii.

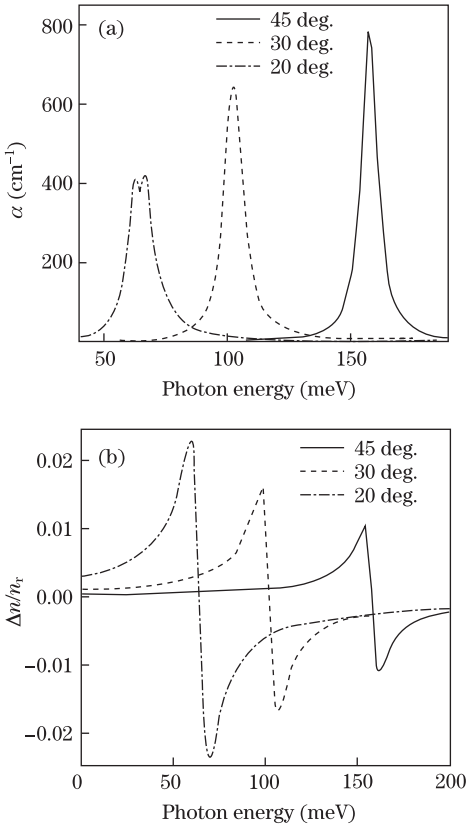

Fig. 5. (a) Total AC and (b) total RI of a CQD versus photon energy for different CQD apex angles.

in the transitions with $\Delta m = 0(\Delta m = \pm 1)$ for $z(x)$-polarization. Thus, given the electromagnetic field polarization and the selection rules, only the transitions with $\Delta m = 0(\Delta m = \pm 1)$ are feasible for $z(x)$-polarization. Moreover, the AC value of 474 cm^{-1} for x-polarization is lower than that of z-polarization because of the smaller transition dipole moment in x-polarization. Figure 7(b) shows that the zero of total RI for x-polarization has a red shift of 62.59 meV.

We aim to further study by considering the Coulomb effects and the alteration of the optical properties.

In conclusion, we obtain the energy levels of a CQD analytically, and subsequently calculate the linear, third-order nonlinear, total ACs, and total RIs. We investigate the effects of the size of QD and the intensity and polarization of the incident electromagnetic field on ACs and RIs. The results show that increasing the size of CQD results in a red shift and in a decrease in total AC or an increase in total RI. As the incident intensity increases, the nonlinear AC and RI increase. Consequently, the total AC and total RI decrease. Therefore, the nonlinear parts should be considered in high-intensity electromagnetic fields. Furthermore, the optical properties of CQD depend on the polarization of the incident field. The peak (zero) of AC(RI) exhibits a red shift because of the shift from the z-direction to the x-direction.

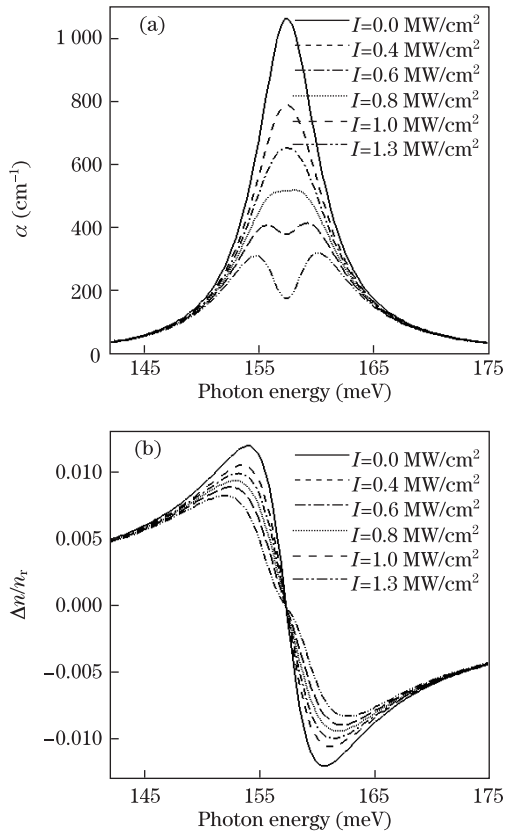

Fig. 6. (a) Total AC and (b) total RI of a CQD versus photon energy for different incident optical intensities.

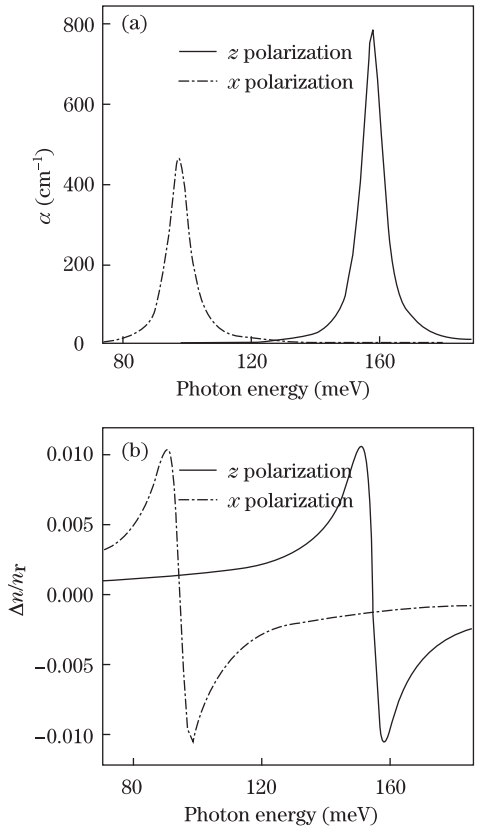

Fig. 7. (a) Total ACs and (b) total RIs of a CQD versus photon energy for electromagnetic fields polarized along the z and x directions.

The authors are grateful to Dr. M. R. K. Vahdani for the relevant ideas.

References

1. S. Ünl ü, İ Karabulut, and H. Şfak, Physica E **33,** 319 (2006).
2. A. Zrenner, J. Chem. Phys. **112,** 7790 (2000).
3. M. R. K. Vahdani and G. Rezaei, Phys. Lett. A **374,** 637 (2010).
4. M. R. K. Vahdani and G. Rezaei, Phys. Lett. A **373,** 3079 (2009).
5. W. Xie, Opt. Commun. **284,** 1872 (2011).
6. W. Xie, Opt. Commun. **284,** 4756 (2011).
7. R. Timm, H. Eisele, A. Lenz, T. Y. Kim, F. Streicher, K. Pötschke, U. W. Pohl, D. Bimberg, and M. Dähne, Physica E **32,** 25 (2006).
8. J. Y. Marzin and G. Bastard, Solid State Commun. **92,** 437 (1994).
9. Y. Li, O. Voskoboynikov, C. P. Lee, and S. M. Sze, Computer Phys. Commun. **141,** 66 (2001).
10. R. V. N. Melnik and M. Willatzen, Nanotechnology **15,** 1 (2004).
11. G. Arfken, *Mathematical Methods for Physicists* (Academic Press, New York, 1970).
12. R. N. Hall, J. Appl. Phys. **20,** 925 (1949).